

Detecting width-wise partial delamination in the composite beam using generalized fractal dimension

S. Keshava Kumar*, Ranjan Ganguli and Dineshkumar Harursampath

Department of Aerospace Engineering, Indian Institute of Science Bangalore, India

(Received January 20, 2016, Revised October 14, 2016, Accepted October 18, 2016)

Abstract. Generalized fractal dimension is used to detect the presence of partial delamination in a composite laminated beam. The effect of boundary conditions and location of delamination on the fractal dimension curve is studied. Appropriability of higher mode shape data for detection of delamination in the beam is evaluated. It is shown that fractal dimension measure can be used to detect the presence of partial delamination in composite beams. It is found that the torsional mode shape is well suited for delamination detection in beams. First natural frequency of delaminated beam is found to be higher than the healthy beam for certain small and partial width delaminations and some boundary conditions. An explanation towards this counter intuitive phenomenon is provided.

Keywords: partial delamination; finite elements; frequency shift; fractal dimension; damage detection

1. Introduction

Fiber reinforced laminated composites are extensively used in aerospace, civil, mechanical and wind energy engineering structures (Della and Shu 2007). Composite laminates are prone to defects such as matrix cracking, strength and stiffness degradation due to aging/corrosion, and delamination between the plies (Zou, Tong *et al.* 2000, Senthil, Arockiarajan *et al.* 2013, Pawar and Ganguli 2003, Gayathri, Umesh *et al.* 2010, Umesh and Ganguli 2009). Delamination in the composite structure may occur either during the manufacturing process or during the service period of the structure. Delamination may not be visible or barely visible to external inspection as delamination is embedded within the composite structures. Delamination caused due to highly concentrated free edge stresses results in the strength degradation of laminates (Chang and Kutlu 1989). Embedded delamination caused by impact, manufacturing defects, or air entrapment, etc, can cause considerable change in the mechanical response of the laminates (Chang and Kutlu 1989). However, delamination reduces the stiffness of the structure and hence it affects the load carrying ability and natural frequencies of the structure (Della and Shu 2007). Structural health monitoring of composite structures becomes necessary to evaluate the integrity and operational limits of the structure in the presence of delamination, as failures of structures, particularly aircraft structures, often have tragic consequences (Zou, Tong *et al.* 2000, Hakim and Razak 2014).

Modeling of composite laminates in the presence of delamination has been extensively studied by many

researchers and is well documented in review articles by Della and Shu (2007), Zou, Tong *et al.* (2000), Chang and Kutlu (1989). Modeling delamination in beams can be approached by two methods. The first method is the region approach of delamination modeling (Della and Shu 2007). The second method is the layer-wise modeling approach (Della and Shu 2007). In the region-wise approach of delamination modeling, the beam is divided into four span-wise regions: two undelaminated regions and two regions in the delaminated segment above and below the delamination interface (Della and Shu 2007). The delaminated region is modeled as two separate sub-beams. The delaminated beam is analyzed as four interconnected beams with suitable boundary conditions at the interface (Della and Shu 2007, Zou, Tong *et al.* 2000). There are two sub-classes of region-based delamination modeling methods, they are the free mode delamination model and the constrained mode delamination model. In free mode delamination model, two sub-beams in the delaminated region deform independently. This leads to impractical elastic curves for certain modes of deformation (Della and Shu 2007). Constrained mode model resolves this issue (Della and Shu 2007). However, these methods of delamination modeling add unnecessary complications and have their own limitations. For instance, the edge delaminated beams cannot be modeled with the above mentioned delamination models. Most of the delamination models for beams, mentioned in the literature, are for beams with through-width delamination; exceptions, which address the issue of beams with partial delamination in the width-wise direction, are restricted to cross-sectional analysis (Guruprasad 2005, Prasad and Harursampath 2012, Venkatesh, Ponnusami *et al.* 2012). However, the delamination model presented by Keshava Kumar *et al.* (Keshava Kumar, Ganguli *et al.* 2013) allows partial width-wise delaminations in beams to be modeled and analyzed.

Nondestructive damage detection methods are

*Corresponding author, Dr.
E-mail: keshav@aero.iisc.ernet.in

categorized into local and global damage identification techniques (Fan and Qiao 2010). Local damage identification techniques use high frequency waves (wavelengths are of the order of thickness of the structure) to detect the damage in the structure (Fan and Qiao 2010). Global damage identification techniques use vibration (wavelengths are of the order of the length of the structure) parameters of the structure. While local damage identification techniques can only indicate the presence and the extent of the damage in the structure, they can seldom quantify the change in structural properties caused by damage. Global damage identification techniques are capable of quantifying the changes in the structural properties. Vibration based damage identification techniques are categorized into a) Frequency domain, b) Time domain, and c) Impedance domain (Zou, Tong *et al.* 2000). Frequency domain damage detection method tracks the changes in the mode shape, mode shape curvature, and frequencies (Hakim and Razak 2014, Xiang *et al.* 2014, Kaveh and Maniat 2015). Time domain damage detection methods use response of the structure to detect damage, and impedance domain uses change in the model damping to detect damage in the structure. Also, vibration based damage identification can be broadly classified into model based method and response based method (Fan and Qiao 2010, Rahmatalla, Eun *et al.* 2012). Model based damage detection of structures is one of the popular methods available (Della and Shu 2007, Zou, Tong *et al.* 2000, Fan and Qiao, 2010). In model based method of damage detection technique, structural model of the healthy as well as the damaged structure properties are used for the damage identification. The presence of delamination reduces the stiffness of the structure, and hence there will be change in the modal parameters of the structures. Therefore, the essence of model-based delamination detection is to capture and amplify the changes in modal parameters of the structure using suitable quantification methods. Though there is ample literature available on mode shape and mode shape curvature based damage detection, there is hardly any literature on small and partial delamination detection in beams using mode shape data. The main reason for this lacuna in the literature is that the delamination causes irregularity of mode shape curves; the extent of the irregularity of the curve depends on the size of delamination (Zou, Tong *et al.* 2000). Small delaminations hardly produce any irregularity in the mode shape (Zou, Tong *et al.* 2000). One of the methods to amplify the small change in mode shape or mode shape curvature is by using Fractal Dimensions(FD).

Fractal dimensions has been used by researchers for the quantification of changes in waveforms. Fractal dimensions have wide applications; some of the practical applications are discussed in chapter 4 of the book by Jefferson and Jarvis (2006). The ways of defining fractals and algorithms for fractal dimension estimation are discussed by Theiler (1990). Katz fractal dimension estimation of waveforms and its usage in detection of waveform anomalies is discussed in articles (Katz 1987, Raghavendra and Dutt 2009, Hadjileontiadis, Douka *et al.* 2005, Qiao, Lestari *et al.* 2007). Katz fractal dimension and other forms of fractal

dimensions – in damage detection of beams and two dimensional structure is used by some researchers in the following articles (Hadjileontiadis, Douka *et al.* 2005, Fan and Qiao 2010, Qiao, Lestari *et al.* 2007, Bai, Song *et al.* 2014, Moustafa and Salamone 2012, Farhidzadeh, Dehghan-Niri *et al.* 2013). Delamination detection in a rotating beam using Katz fractal dimension, and Generalized Fractal Dimension(GFD) was carried out by Keshava Kumar, Ganguli *et al.* (2013, 2015), respectively. Damage detection in plates using Katz fractal dimension is carried out by Hadjileontiadis and Douka (2007), Bai, Ostachowicz *et al.* (2014a). Cao, Ostachowicz *et al.* (2013) have used affine transformation on two dimensional structural mode shape and Katz fractal dimension for damage detection. For mode shapes subjected to noisy data Bai, Ostachowicz *et al.* (2014b) have used scale fractal dimensions to detect crack in a beam. However, Katz fractal dimension may give misleading information when used on higher mode shapes (Wang and Qiao 2007), hence Wang and Qiao (2007) have used Generalized Fractal Dimension (GFD) to detect damage in beams. However, most of the articles detect crack, which is a point phenomenon. A crack behaves as a virtual hinge to larger extent and there will be extensive change in modal parameters of the structure. Hence, detecting the crack will be relatively simpler compared to the delamination, as delamination is a distributed phenomenon and with the presence of partial delamination changes in the modal parameters are abysmal. The article by Wang and Qiao (2007) uses full width delamination model. The sensitivity of the fractal dimension curve for small and partial width delamination is not accounted in their study. The width-wise partial delamination in beams will lead to coupling to bending-torsion mode coupling, and the effect this mode shape coupling and the effect of different boundary conditions on detecting, locating and sizing of the delamination is seldom studied. From the literature review on delamination detection; it is clear, that the emphasis has been on the full-width delamination detection. However, width-wise edge and partial delamination detection in helicopter rotor blade and wind turbine blade is a major concern. Hence, the main aim of the article is to study the capability of GFD to capture width-wise partial delamination in laminated composite beams.

The contributions of the present article are: to detect width-wise partial and length-wise small delamination in laminated composite beams; the usage of GFD on first few mode shapes to detect and locate delamination; and, explore torsional mode shape for delamination detection. Apart from the above mentioned major contributions, following observations and contributions are made in the article. Effect of the boundary conditions and delamination location on the fractal dimension curves is analyzed. First natural frequency of delaminated beam is found to be higher for some boundary conditions, for certain small and partial width delaminations. A mathematical explanation for this counter intuitive phenomenon is presented in the article. Finally, it is shown that the torsional mode shape is best suited for partial delamination detection in composite beams.

2. Kinematics and energy

The composite beam and the co-ordinate system considered are shown in Fig. 1. In the figure, L represents the length of the beam, B is the width of the beam, and $2h$ is the thickness of the beam. The delamination is located at a distance of X_d in the lengthwise direction (X direction) of the beam, and the length of the delamination is l_d . In the widthwise direction of the beam cross section, that is in the Y direction, a delamination length of $2b_2$ to the left of the beam cross section (negative Y direction) and a delamination length of $2b_4$ to the right of the beam cross section (positive Y direction) are considered as shown in Fig. 2. The delamination at the left of the beam cross section, starts at $-Y_l^d$ and ends at $-Y_l^h$, and the delamination on the right of the beam cross section, starts at Y_r^d and exists up to the tip of the beam cross section. In the thickness direction of the beam cross section, delamination is at a distance of Z_l^d from the mid-plane on the left side, and on the right side of the beam the delamination is located at $Z = -Z_r^d$. The delaminated beam cross section is partitioned into sub-sections 1 to 6, indicated by corresponding encircled numbers in Fig. 2, for the ease of energy calculation. The local coordinate system for the sections are shown in Fig. 2.

2.1 Assumptions

Following assumptions are made for the displacement-based formulation of the beam.

- The plane section normal to the center line of the beam, remains plane after deformation (Reddy 1997).
- Through-the-thickness deformation and stresses are negligible (Jones 1999).
- Beam bending is predominantly in $X-Z$ plane.
- The warping in cross-section of the beam is ignored.

2.2 Displacement fields

Adopting the displacement field assumed in (Jun, Hongxing *et al.* 2008) and accounting for the displacement of material points of the cross-section due to torsion as well, the following expressions are obtained

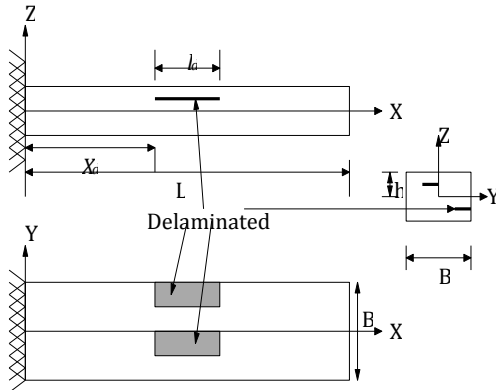


Fig. 1 Dimensions and cross section of beam with delamination

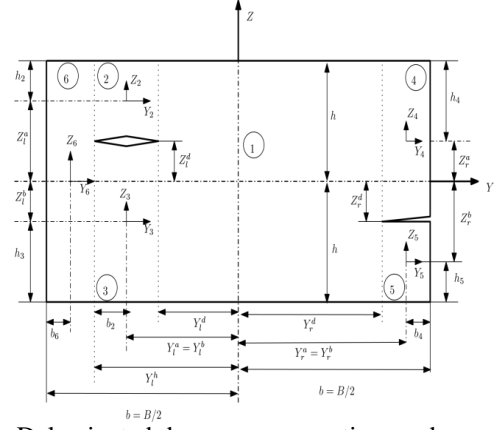


Fig. 2 Delaminated beam cross section and coordinated systems

$$u(X, Y, Z, t) = u_0(X, t) + Z \theta(X, t) \quad (1)$$

$$v(X, Y, Z, t) = -Z \psi(X, t) \quad (2)$$

$$w(X, Y, Z, t) = w_0(X, t) + Y \psi(X, t) \quad (3)$$

Here, w_0 is the transverse displacement of material points in the mid-plane, u_0 is the axial displacement of material points in the mid-plane, θ is the rotation of the cross-section about Y axis, and ψ is the rotation of cross-section about X -axis. Independent spatial variables are X , Y , and Z , and t is the temporal variable.

2.3 Displacement field in the delaminated region

Partially delaminated beam cross-section considered is shown in Fig. 2. The delaminated beam cross-section is partitioned into six regions as depicted in Fig. 2. This particular configuration of delamination and partitioning of the cross-section of the beam is ideal to simulate most of the delamination cases arising in beam-like structures.

The displacement function for u of the delaminated cross-sections in the region $x_d < X < x_d + l_d$ of the beam is piecewise continuous, and is given by Eq (4). The assumptions and reasoning behind arriving at the displacement function u in the delaminated region is explained by the same authors in article (Keshava Kumar, Ganguli *et al.* 2013).

(X, Y, t)

$$= \begin{cases} u_0(X, Z, t) + Z \theta & \forall -h \leq Z \leq h \text{ and } -Y_l^d \leq Y \leq Y_r^d \\ u_0 + Z_1^d [m_{df} \phi(Y_2)] + Z_2 \theta & \forall -h_2 \leq Z_2 \leq h_2 \text{ and } -b_2 \leq Y_2 \leq b_2 \\ u_0 - Z_1^b [m_{df} \phi(Y_3)] + Z_3 \theta & \forall -h_3 \leq Z_3 \leq h_3 \text{ and } -b_2 \leq Y_3 \leq b_2 \\ u_0 + Z_r^a [m_{df} \phi(Y_4)] + Z_4 \theta & \forall -h_4 \leq Z_4 \leq h_4 \text{ and } -b_4 \leq Y_4 \leq b_4 \\ u_0 - Z_r^b [m_{df} \phi(Y_5)] + Z_5 \theta & \forall -h_5 \leq Z_5 \leq h_5 \text{ and } -b_4 \leq Y_5 \leq b_4 \end{cases} \quad (4)$$

The factor $m_{df} \phi(Y)$ is a function, which specifies the amplification of the displacement in the delaminated region due to the delamination, or equivalently the reduction in stiffness of the delaminated region due to the delamination.

$$m_{df} = 1 - (l_{dr})^m * (1 - w_{dr})^n m_{df} = 1 - \sin\left(\frac{\pi d_r}{2}\right) * \left[1 - \cos\left(\frac{\pi d_r}{2}\right)\right]^2 \quad (5)$$

Here $m = 1$ and $n = 2$ is used in arriving at the delaminated cross-sectional stiffness for beams with cantilever and simply supported boundary conditions. Trigonometric modification factor of Eq. (5) is used for beam subjected to fixed-fixed boundary condition. The reason behind using different modification factor functions for beams subjected to different boundary conditions is explained in the article (Keshava Kumar, Ganguli *et al.* 2013).

The function $\phi(Y)$ is to be chosen so that the stresses σ_x and τ_{xy} are continuous at the interface of sections 1-2, 1-3, 1-4, 1-5, 2-6, and 3-6. The variation of the stress at the interface of the healthy and delaminated section in the widthwise direction may be something similar to stress concentration at the tip of the notch in an isotropic plate. Contribution of $\phi(Y_2)$ to the cross-sectional stiffness terms will be negligible and hence $\phi(Y_2) = 1$ can be considered in calculating the cross-sectional stiffness; but if the intention is to obtain stresses and axial displacement at the interface of healthy and delaminated beam segments, then a suitable function for $\phi(Y_2)$ has to be assumed or derived. Researchers are referred to article (Keshava Kumar, Ganguli *et al.* 2013) for more detailed discussion on $\phi(Y)$. Article by Kornev, Kurguzov *et al.* (2012) details out - how to calculate stresses at the junction of delaminated and healthy segment of the beam and the growth of delamination based on the stress distribution at the delaminated and healthy structure interface.

2.4 Strain, curvature, displacement relation

Non-zero strains in the beam are obtained from the above displacement field as

$$\begin{aligned} \varepsilon_{xx} &= \frac{\partial u}{\partial X} = \frac{\partial u_0}{\partial X} + Z \frac{\partial \theta}{\partial X} \\ \gamma_{xz} &= \frac{\partial u}{\partial Z} + \frac{\partial w}{\partial X} = \frac{\partial w}{\partial X} + \theta \\ \gamma_{xy} &= -Z \frac{\partial \psi}{\partial X} \end{aligned} \quad (6)$$

Mid-plane strains and curvatures are

$$\begin{aligned} \varepsilon_{xx}^0 &= \frac{\partial u_0}{\partial X} \\ \kappa_x &= \frac{\partial \theta}{\partial X} \\ \kappa_{xy} &= \frac{\partial \psi}{\partial X} \end{aligned} \quad (7)$$

2.5 Stresses and energy

From classical laminate plate theory (CLPT), the stresses in the lamina (Jones 1999) are given by

$$\begin{Bmatrix} \sigma_x \\ \sigma_y \\ \tau_{xy} \end{Bmatrix} = \begin{bmatrix} \bar{Q}_{11} & \bar{Q}_{12} & \bar{Q}_{16} \\ \bar{Q}_{12} & \bar{Q}_{22} & \bar{Q}_{26} \\ \bar{Q}_{16} & \bar{Q}_{26} & \bar{Q}_{66} \end{bmatrix} \begin{Bmatrix} \varepsilon_x \\ \varepsilon_y \\ \gamma_{xy} \end{Bmatrix} \quad (8)$$

For bending of beams predominantly in $X-Z$ plane, resulting from the applied force and moment in $X-Z$ plane, the normal stress σ_y is equal to zero, while the strain ε_y in composite beam may not be zero due to Poisson effect (Jun, Hongxing *et al.* 2008).

Thus stresses in a lamina of the beam are

$$\begin{Bmatrix} \sigma_x \\ \tau_{xy} \end{Bmatrix} = \begin{bmatrix} \tilde{Q}_{11} & \tilde{Q}_{16} \\ \tilde{Q}_{16} & \tilde{Q}_{66} \end{bmatrix} \begin{Bmatrix} \varepsilon_x \\ \gamma_{xy} \end{Bmatrix} \quad (9)$$

where, $\tilde{Q}_{11} = \bar{Q}_{11} - (\bar{Q}_{12})^2 / \bar{Q}_{22}$, $\tilde{Q}_{16} = \bar{Q}_{16} - (\bar{Q}_{12} * \bar{Q}_{26}) / \bar{Q}_{22}$ and $\tilde{Q}_{66} = \bar{Q}_{66} - (\bar{Q}_{26})^2 / \bar{Q}_{22}$, and \bar{Q}_{ij} 's are transformed lamina stiffness coefficients (Jones 1999). In CLPT, the laminae are assumed to be in a state of plane stress and hence the shear stress in the $X-Z$ plane is not considered, but in the case of Timoshenko beam theory, we do have shear stress in the thickness direction. Fortunately, for orthotropic laminae, shear-extension coupling coefficients are not present and hence shear stress in the $X-Z$ plane is given by $\tau_{xz} = \bar{Q}_{55} \gamma_{xz}$.

Torsion induces shear stress τ_{xy} and τ_{yz} in the beam. The expression for shear stresses τ_{xy} and τ_{yz} has to be obtained using membrane analogy, as discussed by Swanson (1998). Contribution of shear stress τ_{yz} towards the torsional rigidity of the beam, for thin-walled beams is negligible and hence can be neglected (Swanson 1998). Presence of delamination in the beam will shift the shear center of the beam cross-section in the delaminated segment; the shift in the shear center of the delaminated beam segment can be obtained by following the formulation similar to thin-walled beam cross-sections as suggested by some researchers (Lee 2001, Lee and Kim 2001, Sheik and Thomsen 2008). The cross-sectional stiffness terms of the delaminated beam segment corresponding to torsional rigidity can be obtained by means followed by Sheik and Thomsen (2008), Lee and Kim (2001).

The strain energy in the beam is given by

$$V = \frac{1}{2} \int_0^L \int_{-B/2}^{B/2} \int_{-h}^h \{\sigma\}^T \{\varepsilon\} dZ dY dX \quad (10)$$

$$V = \frac{1}{2} \left\{ \int_0^{X_d} \{\bar{\varepsilon}\}^T [D] \{\bar{\varepsilon}\} dX + \int_{X_d}^{(X_d+l_d)} \{\bar{\varepsilon}\}^T [D] \{\bar{\varepsilon}\} dX + \int_{(X_d+l_d)}^L \{\bar{\varepsilon}\}^T [D] \{\bar{\varepsilon}\} dX \right\} \quad (11)$$

where

$$\{\sigma\} = \begin{Bmatrix} \sigma_x \\ \tau_{xy} \\ \tau_{xz} \end{Bmatrix}; \{\varepsilon\} = \begin{Bmatrix} \varepsilon_{xx} \\ \gamma_{xy} \\ \gamma_{xz} \end{Bmatrix}; \{\bar{\varepsilon}\} = \begin{Bmatrix} \varepsilon_{xx}^0 \\ \gamma_{xz} \\ \kappa_x \\ \kappa_{xy} \end{Bmatrix} \quad (12)$$

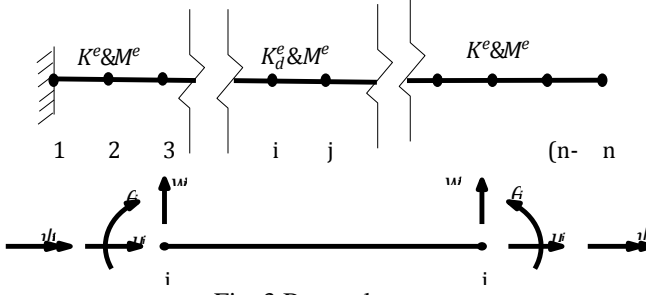


Fig. 3 Beam element

$$[D] = \begin{bmatrix} \bar{A}_{11} & 0 & \bar{B}_{11} & \bar{B}_{16} \\ 0 & \bar{A}_{55} & 0 & 0 \\ \bar{B}_{11} & 0 & \bar{D}_{11} & \bar{D}_{16} \\ \bar{B}_{16} & 0 & \bar{D}_{16} & \bar{D}_{66} \end{bmatrix}; [D]_d = \begin{bmatrix} \bar{A}_{11}^d & 0 & \bar{B}_{11}^d & \bar{B}_{16}^d \\ 0 & \bar{A}_{55} & 0 & 0 \\ \bar{B}_{11}^d & 0 & \bar{D}_{11}^d & \bar{D}_{16}^d \\ \bar{B}_{16}^d & 0 & \bar{D}_{16}^d & \bar{D}_{66}^d \end{bmatrix} \quad (13)$$

$$\bar{A}_{11} = B \int_{-h}^h \bar{Q}_{11} dZ \quad \bar{A}_{55} = B k_s \int_{-h}^h \bar{Q}_{55} dZ \quad \bar{B}_{11} = B \int_{-h}^h \bar{Q}_{11} Z dZ$$

$$\bar{B}_{16} = B \int_{-h}^h \bar{Q}_{16} Z dZ \quad \bar{D}_{11} = B \int_{-h}^h \bar{Q}_{11} Z^2 dZ \quad \bar{D}_{16} = B \int_{-h}^h \bar{Q}_{16} Z^2 dZ$$

$$\bar{D}_{66} = 4B \int_{-h}^h \bar{Q}_{66} Z^2 dZ$$

Here k_s is the shear correction factor.

Kinetic energy of the laminated composite beam is

$$T = \frac{1}{2} \int_0^L \int_{-h}^h \rho^k \left[\left(\frac{\partial u}{\partial t} \right)^2 + \left(\frac{\partial v}{\partial t} \right)^2 + \left(\frac{\partial w}{\partial t} \right)^2 \right] B dZ dX$$

where ρ^k is the density of the equivalent homogenized material constituting the k^{th} lamina. The delaminated cross section stiffness coefficients and complete representation of kinetic energy can be referred in article (Keshava Kumar, Ganguli *et al.* 2013).

3. Beam element

The finite element model for the composite beam consists of two noded and four degrees of freedom (DOF) per node element. The DOF at each node are: axial displacement u , transverse displacement w , slope θ , and twist ψ . C^0 shape functions are considered for the axial displacement and the twist, shape functions for transverse displacement and slope are obtained from the Timoshenko functions (C^1 type). C^1 type shape functions for Timoshenko beam element are prone to shear locking phenomenon, but by using Timoshenko functions the phenomenon of shear locking can be avoided (Lin and Zhang 2011). Finite element discretization of the beam is

shown in Fig. 3. K^e mentioned in the figure, denotes the healthy composite beam element stiffness matrix, and M^e stands for the mass matrix of the composite beam element. K_d^e denotes the delaminated beam element stiffness matrix. The mass matrix of the delaminated beam is considered to be same as that of healthy beam, as there will be hardly any loss of material or any significant changes in the cross-section due to delamination.

3.1 Shape functions

Shape functions for axial displacements and twist of the composite laminated beam are given by Eq. (14), where x is the local co-ordinate system and l_e is the element length.

$$N_1^u = 1 - \frac{x}{l_e} \quad (14)$$

$$N_2^u = \frac{x}{l_e}$$

The shape functions for the transverse displacements based on the Timoshenko displacement functions (Lin and Zhang 2011) or equivalently from the interdependent interpolation element of (Reddy 1997) are

$$N_1^b = 1 + \frac{2\mu_e x^3}{l_e^3} - \frac{3\mu_e x^2}{l_e^2} + \left(\frac{\mu_e - 1}{l_e} \right) x$$

$$N_2^b = \frac{\mu_e x^3}{l_e^3} - \frac{(3\mu_e + 1)x^2}{2l_e} + \left(\frac{\mu_e + 1}{2} \right) x$$

$$N_3^b = -\frac{2\mu_e x^3}{l_e^3} + \frac{3\mu_e x^2}{l_e^2} - \left(\frac{\mu_e - 1}{l_e} \right) x$$

$$N_4^b = \frac{\mu_e x^3}{l_e^3} + \frac{(1 - 3\mu_e)x^2}{2l_e} + \left(\frac{\mu_e - 1}{2} \right) x \quad (15)$$

The shape functions for the rotation based on the Timoshenko displacement functions (Lin and Zhang 2011) or equivalently from the interdependent interpolation element of (Reddy 1997) are

$$N_1^s = -\frac{6\mu_e}{l_e^2} + \left(\frac{x^2}{l_e} - x \right)$$

$$N_2^s = -1 - \frac{3\mu_e x^2}{l_e^2} + \left(\frac{3\mu_e + 1}{l_e} \right) x$$

$$N_3^s = \frac{6\mu_e x^2}{l_e^2} - \frac{6\mu_e}{l_e^2} x$$

$$N_4^s = -\frac{3\mu_e x^2}{l_e^2} - \left(\frac{1 - 3\mu_e}{l_e} \right) x \quad (16)$$

Here, $\mu_e = 1/(1+12\lambda e)$ and $\lambda_e = \frac{\bar{D}_{11}}{A_{55}L^2}$ where L is the length of the beam, B is the width of the beam, l_e is the element length, h is the semi-thickness of the beam, and x is the element's local coordinate. The advantage of the above interdependent interpolation shape functions is that by considering $\mu_e = 1$ and shear correction factor $k_s=0$, the Timoshenko beam model reduces to Euler-Bernoulli beam finite element model.

The displacements for the composite beam element in

the form of nodal displacements, are now given by

$$\begin{Bmatrix} u^0(x) \\ w^0(x) \\ \theta(x) \\ \psi(x) \end{Bmatrix} = \begin{bmatrix} N_1^u & 0 & 0 & 0 & N_2^u & 0 & 0 & 0 \\ 0 & N_1^b & N_2^b & 0 & 0 & N_3^b & N_4^b & 0 \\ 0 & N_1^s & N_2^s & 0 & 0 & N_3^s & N_4^s & 0 \\ 0 & 0 & 0 & N_1^u & 0 & 0 & 0 & N_2^u \end{bmatrix} \begin{Bmatrix} u_1 \\ w_1 \\ \theta_1 \\ \psi_1 \\ u_2 \\ w_2 \\ \theta_2 \\ \psi_2 \end{Bmatrix} \quad (17)$$

The above equation can be represented in compact form as, $\{\tilde{q}\} = [N]\{q_e\}$, where $[N]$ is shape function matrix, and $\{q_e\}$ is the nodal displacement vector.

4. Governing equations

The finite element equations of the system are derived by using Hamilton's principle, which is stated as

$$\int_{t_1}^{t_2} \sum_{e=1}^N (\delta T^e - \delta V^e) dt = 0 \quad (18)$$

Where, t_1 and t_2 are the initial and final times respectively, and the variations of displacements at initial and final time step is considered to be zero, i.e. $\delta u_0 = \delta w_0 = \delta \theta = \delta \psi = 0$ at $t = t_1, t_2$, in the equation derivation. δT_e is variation in the kinetic energy and δV_e is the variation of strain energy of the element.

Finite element equation for the eigenvalue problem is obtained as

$$Kq = \omega^2 Mq \quad (19)$$

There are many methods for solving the above eigenvalue problem (Bathe 1982, Chandrupatla and Belegundu 2002). The inverse iteration method and generalized Jacobi method are the simplest and widely used for small number of degree of freedom systems (Chandrupatla and Belegundu 2002). Since our problem is a simple beam, we have used the above mentioned methods.

5. Fractal dimensions and damage detection

Fractal dimension measures the complexity in a signal. Fractal dimension gives a non-integer dimension for the waveform, which is always greater than one. Fractal dimension of the building block of a fractal or waveform; and the fractal dimension of the complete waveform or fractal, should be the same. Delamination in the structure will affect the stiffness of the structure, which in-turn will result in slight change in the mode shape. Evaluating fractal dimensions on the mode shape data will amplify the slight localized changes in the curve and will help in detecting and locating the delamination.

Fractal dimension of a curve as defined by Katz (1987) is

$$FD = \frac{\log_{10}(n)}{\log_{10}\left(\frac{d}{l}\right) + \log_{10}(n)} \quad (20)$$

Here, l is the total length of the curve, d is the planar extent of the curve and n is the number of steps in the curve (Katz 1987). However, Katz fractal dimension when used on higher mode shapes may give misleading information (Wang and Qiao 2007). To avoid the difficulty caused by FD, FD algorithm is modified by introducing a scale parameter S , and the modified FD is called generalized fractal dimension (Wang and Qiao 2007).

$$GFD = \frac{\log_{10}(n)}{\log_{10}\left(\frac{d_s}{l_s}\right) + \log_{10}(n)} \quad (21)$$

$$d_s = \max_{1 \leq j \leq n} \sqrt{[y(x_{i+j}) - y(x_i)]^2 + S^2(x_{i+j} - x_i)^2}$$

$$l_s = \sum_{j=1}^n \sqrt{[y(x_{i+j}) - y(x_i)]^2 + S^2(x_{i+j} - x_i)^2}$$

Where, x_i is the starting node of the window, x_{i+j} distance of the $(i+j)^{th}$ node, and $y(x_i)$ is the normalized modal displacement at i^{th} node. Fig. 4 illustrates the window, nodal co-ordinate nomenclature and node numbering scheme used in fractal dimension calculation. Scale parameter S can take any value, but $S = 100$ is used in the present article to calculate generalized fractal dimension.

6. Results and discussion

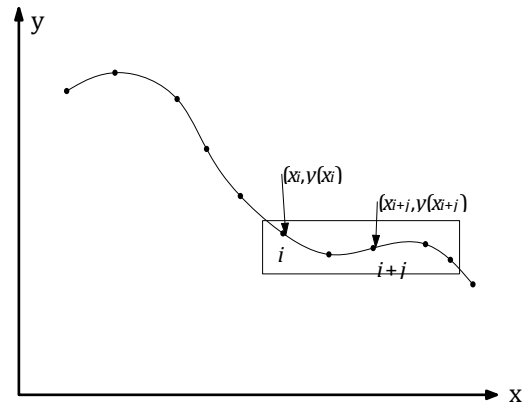


Fig. 4 Illustration of a fractal dimension window

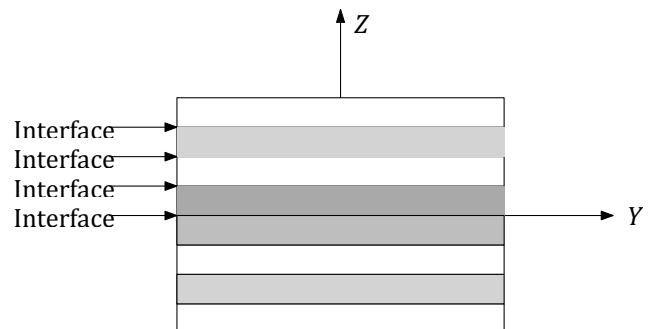


Fig. 5 Delamination considered at different interfaces

Table 1 Natural frequencies (Hz) for 25.4mm delamination length for cantilever beam

	Experimental (Shen and Grady 1992)	FSDT (Shen and Grady 1992)	3D FEM	Present m=1,n=2
Healthy	79.88, 79.75, 79.88	82.04	81.46	81.17
Interface 1	78.38, 79.13, 77.00	80.13	81.43	79.87
Interface 2	78.38, 76.63, 78.38	81.39	76.04	74.39
Interface 3	79.63, 80.13, 80.63	81.46	67.37	62.90
Interface 4	75.32, 75.25, 77.25	81.60	53.65	47.98

A cantilever beam made of graphite/epoxy composite with stacking sequence $[0/90]_{2s}$, 0.127 m length, 0.0127 m breadth, and 1.016 mm thickness, is considered for the numerical simulation for the healthy as well as delaminated states of the beam. Each ply has a thickness of 0.127 mm. This particular configuration of the beam is used in simulation, as experimental, analytical and numerical results are available in the literature (Shen and Grady 1992) for comparison. This beam is used by many researchers to validate their results. Different delamination lengths are considered in the simulation. Delamination in the thickness direction is considered at different interfaces shown in Fig. 5. The beam is meshed with equi-sized elements. The natural frequency for a cantilevered healthy beam as well as for the full-width delaminated states of the beam obtained from the delaminated beam element are compared with literature (Shen and Grady 1992) and/or with the 3D finite element simulation. The results for the beam with 25.4 mm delamination length at different interfaces are tabulated in Table 1. The results for the beam with 50.8 mm delamination length at different interfaces are tabulated in Table 2.

The effect of boundary condition and delamination length on the first natural frequency of the beam are tabulated in Table 3. In Table 3 acronym 'C' stands for cantilever boundary condition, 'SS' stands for simply supported boundary condition, and 'FF' stands for fixed-fixed boundary condition.

Results in Table 3 show natural frequency of the delaminated beam for certain delamination length and boundary condition is higher than the natural frequency of the healthy beam. This phenomenon is counter intuitive, as delamination results in reduction in stiffness, but the natural frequency is higher. Delaminated structures in-fact can have higher frequency depending on the boundary conditions, size of delamination, location of delamination and the mode shape under consideration.

This phenomenon is also observed by the researchers Tracy and Pardoen (1989), Hou and Jeronimidis (1999). It can also be explained mathematically as follows: eigenvalue problem from the FE free vibration context is defined as

Table 2 Natural frequencies (Hz) for 50.8mm delamination length for cantilever beam

	Experimental (Shen and Grady 1992)	FSDT DT	FE-FS	3D FEM	Present m=1, n=2
Healthy	79.88, 79.75, 79.88	82.04	82.00	81.46	81.17
Interface 1	74.38, 75.00, 76.75	75.29	76.52	76.04	74.39
Interface 2	75.13, 75.25, 75.00	78.10	77.02	79.11	74.58
Interface 3	79.50, 81.88, 77.88	79.93	80.56	78.58	77.21
Interface 4	69.38, 68.00, 69.38	80.38	80.64	80.28	77.56

Table 3 Effect of delamination at interface 1 on first three natural frequencies (Hz)

l_d	BC	3D FEM	Present m=1, n=2
Healthy	C	81.46	81.17
	SS	229.10	227.86
	FF	507.99	516.54
25.4mm	C	81.43	79.87
	SS	229.14	225.04
	FF	514.84	521.27
50.8mm	C	76.04	74.39
	SS	228.44	198.31
	FF	513.76	509.46

$$[K]x = \lambda_i [M]x \quad (22)$$

where, $[K]$ and $[M]$ are $n \times n$ stiffness and mass matrices respectively, and x is the $n \times 1$ displacement vector. Let, λ_i be the eigenvalues of the system and φ_i be the mass normalized eigenvector of the system. where index i takes values from 1 to n .

Considering healthy and delaminated systems, the system equations can be written as

$$[K_h]\varphi_i = \lambda_i [M]\varphi_i \quad (23)$$

$$[K_d]\tilde{\varphi}_i = \lambda_i [M]\tilde{\varphi}_i \quad (24)$$

Since, there is negligible mass loss due to delamination, mass matrix of both systems would be same. Subscript h stands for healthy system and subscript d stands for the delaminated system. Eigenvectors of both the systems are mass normalized. Degradation of stiffness due to delamination means for any given vector Φ

$$\Phi^T [K_h] \Phi > \Phi^T [K_d] \Phi \quad (25)$$

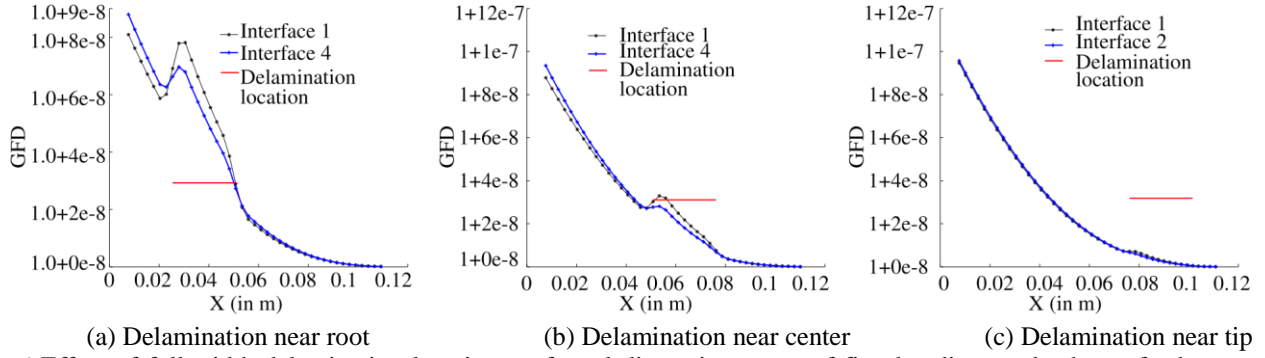


Fig. 6 Effect of full-width delamination location on fractal dimension curve of first bending mode shape, for beam with cantilever boundary condition

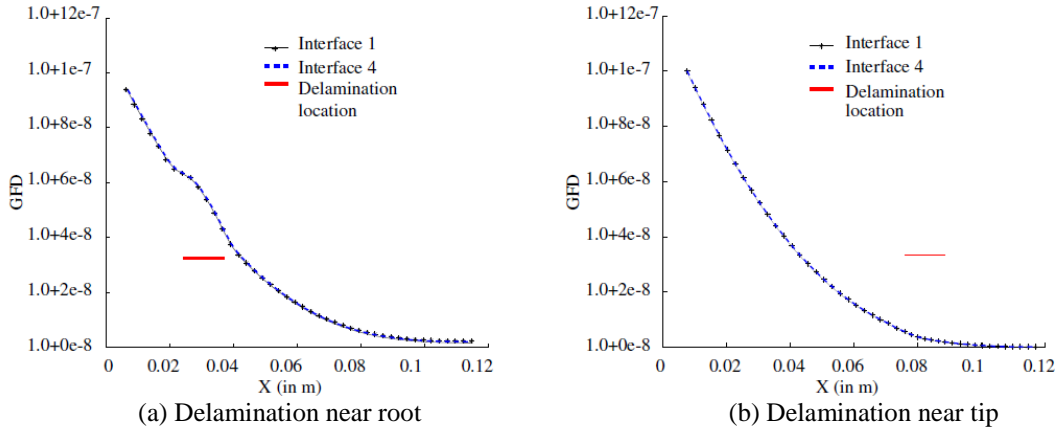


Fig. 7 GFD of first bending mode of cantilever beam with partial width delamination

Premultiplying the Eq. (23) by φ_i^T and Eq. (24) by $\tilde{\varphi}_i^T$, we get

$$\varphi_i^T [K_h] \varphi_i = \lambda_i \varphi_i^T [M] \varphi_i \quad (26)$$

$$\tilde{\varphi}_i^T [K_d] \tilde{\varphi}_i = \tilde{\lambda}_i \tilde{\varphi}_i^T [M] \tilde{\varphi}_i \quad (27)$$

Dividing Eq. (27) by Eq. (26), we get

$$\frac{\tilde{\varphi}_i^T [K_d] \tilde{\varphi}_i}{\varphi_i^T [K_h] \varphi_i} = \frac{\tilde{\lambda}_i}{\lambda_i} \quad (28)$$

From the above equation, it is clear that for small delaminations with favorable eigenvectors, $\frac{\tilde{\lambda}_i}{\lambda_i}$ can be greater than 1. In short $\tilde{\lambda}_i < \lambda_i$, if and only if $\varphi_i = \tilde{\varphi}_i$ and $\tilde{\varphi}_i^T [K_d] \tilde{\varphi}_i < \varphi_i^T [K_h] \varphi_i$, otherwise $\tilde{\lambda}_i$ can be greater than, or equal to, or less than λ_i . This phenomenon of higher first natural frequency of the delaminated beam as compared to a healthy beam, is also seen in the articles Tracy and Pardoen (1989), Hou and Jeronimidis (1999). This phenomenon can also be looked at from the perspective of redistribution of energy into different mode shapes upon delamination. Upon delamination, first mode shape of the delaminated beam may share higher energy as compared to that of a healthy beam.

6.1 Fractal dimension of mode shape

Calculation of fractal dimension requires three parameters: (1) length of the curve, (2) distance between the end points of the curves, and (3) number of segments used to represent the curve. The objective here is to locate the delamination in the structure. Fractal dimension can be calculated for a segment of the curve and this number can be assigned to the midpoint of the segment. In a similar fashion, fractal dimension for the whole curve is calculated in a segment wise fashion.

To have a better resolution, there will be overlap between the neighboring segments, but the overlap will always be less than 100 percent. The values of fractal dimension calculated are plotted as a curve along the length of the beam and delamination presence and location is interpreted based on the changes seen in the fractal dimension curve. Fractal dimension is calculated for the normalized mode shape, by considering a window (segment) of five nodes or four elements and the calculated fractal dimension is assigned to the mid-node of the window (Hadjileontiadis, Douka *et al.* 2005). This window is slid to encompass the next node plus the previous four nodes. This process is repeated to cover entire length of the beam. The fractal dimension is calculated for each and every node of the beam, except for the first and the last two nodes of the beam. The selection of four elements in calculating fractal dimension is empirical in nature

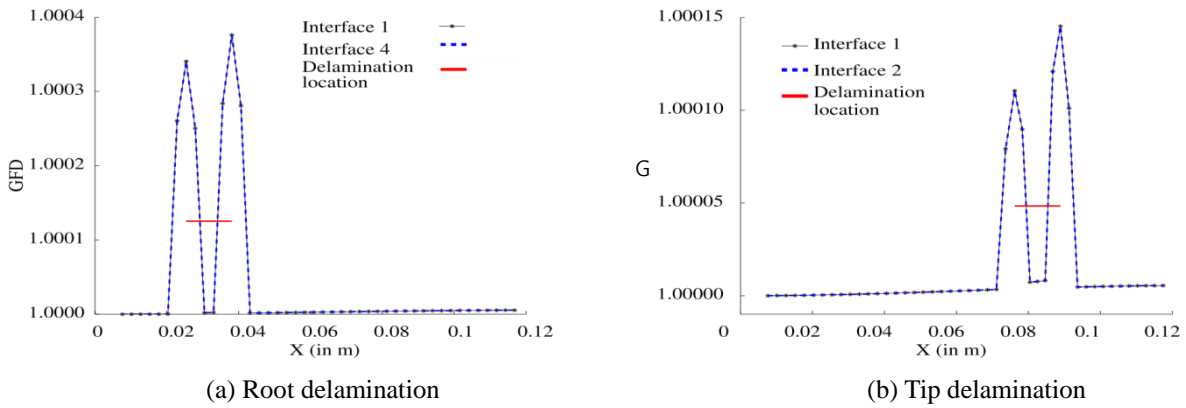


Fig. 8 GFD of first torsional mode of cantilever beam with partial width delamination

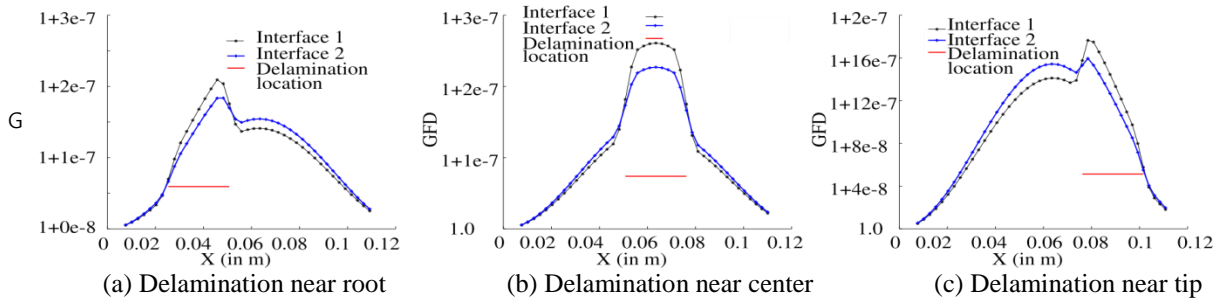


Fig. 9 Effect of simply supported boundary condition for full-width delamination, on the fractal dimension curve of first bending mode shape

(Hadjileontiadis, Douka *et al.* 2005). Using more number of elements in a segment requires either using more elements in the total beam length in the simulation, or in experiments it requires more sampling points. Using less number of elements i.e. less than four elements per window may be susceptible to noise if used on experimental data (Hadjileontiadis, Douka *et al.* 2005).

6.2 Cantilever boundary condition

In this section, we investigate the use of generalized fractal dimension for full width and partial width delamination detection.

6.2.1 Full width delamination

Fractal dimension curve obtained using mode shape data of the full width delaminated beam with fixed-free (cantilever) boundary condition is plotted in Fig. 6. The delamination length considered for simulation is 25.4 mm. Horizontal line in Fig. 6 is the length and location of delamination. The change in the fractal dimensions due to shift in delamination location in the thickness direction i.e. at different interfaces (refer Fig. 5) is plotted in Fig. 6. Though there is a difference in the values of fractal dimension for delamination at different interfaces, we cannot conclusively say what value of fractal dimension refers to location of delamination in the thickness direction.

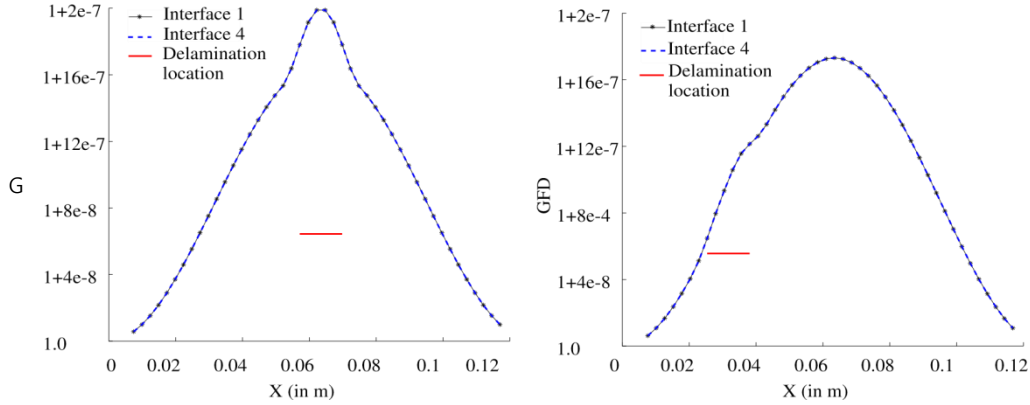
However, we can conclusively locate the presence of delamination in the laminate, in the length-wise direction. Though the fractal dimension values at the root of the beam are higher than the fractal dimension values at the delamination location of the beam, but the variation in fractal dimension curve at delamination location is a clear indicative of presence of delamination.

The effect of change in the location of the delamination in the length-wise direction on fractal dimension is plotted in Figs. 6(a) to 6(c). The location of the delamination in the beam is shown by a horizontal line in the figures.

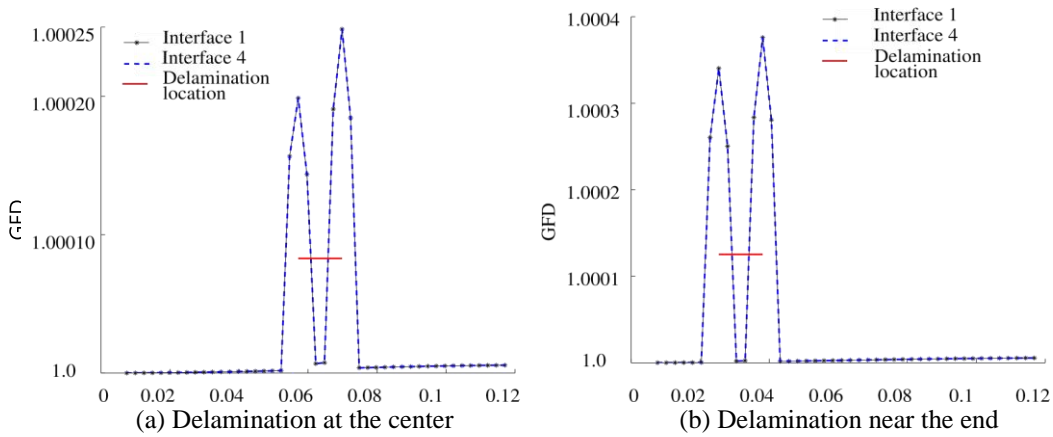
6.2.2 Partial width delamination

Full-width delamination in beams could be detected using fractal dimension method by using first mode shape data. The stiffness degradation of partially delaminated beam is meager when compared to full width delaminated beam. The capability of fractal dimension to detect partial delamination in beams is evaluated in this section. Fig. 7 is the fractal dimension plot for 12.5 mm length delamination and 50 percentage of width delamination, location of delamination in the length-wise direction is shown in the Fig. 7 by a horizontal line. Presence of delamination near the root can be detected as there is variation in the curve, but for the delamination location near the tip the curve blip is not conclusive enough (refer Fig. 7(b)).

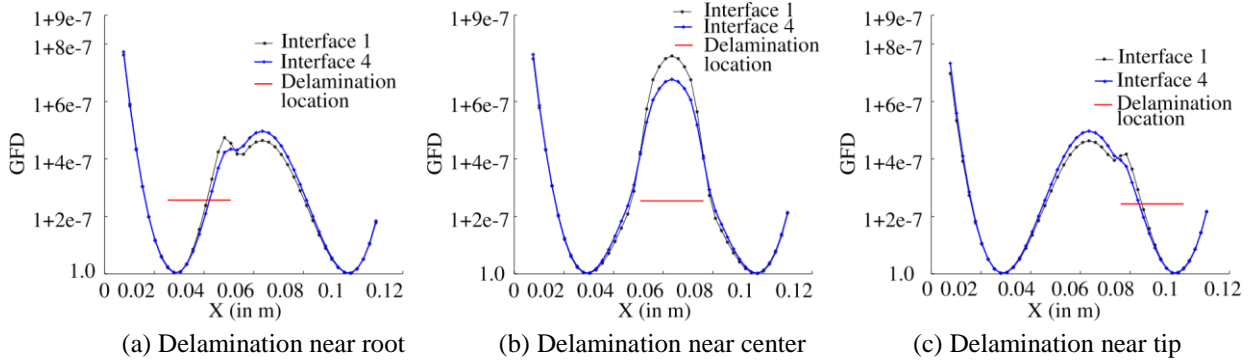
Fractal dimension curve for the first bending mode shape of the partial delaminated cantilever beam did not yield conclusive evidence for the presence of delamination



(a) Delamination at the center (b) Delamination near the end
 Fig. 10 GFD of first bending mode for partial width delamination in simply supported beam



(a) Delamination at the center (b) Delamination near the end
 Fig. 11 GFD of first torsion mode for simply supported beam



(a) Delamination near root (b) Delamination near center (c) Delamination near tip
 Fig. 12 Effect of full width delamination on the generalized dimension curve of first bending mode for fixed-fixed boundary condition

at the tip of beam. Hence to detect partial delamination in the beam, higher mode shape data is used. Torsional mode shapes are sensitive to delamination and for the present beam configuration and delamination, third mode shape of the beam corresponds to the torsional mode shape of the beam. Torsional mode shape data is now used for the calculation of fractal dimension curve. Fig. 8 is the fractal dimension plot for 12.5 mm length delamination and 50 percentage of width delamination, location of delamination in the length-wise direction is shown in the Fig. 8 by a horizontal line. The presence of the delamination can be

clearly identified by looking at the peaks in the fractal dimension curves. Torsional mode shape fractal dimension curves are conclusive enough to detect partial width delamination at different locations of delamination along the length of the beam.

6.3 Simply supported boundary condition

The effect of simply supported boundary condition and the location of the delamination on the fractal dimension curve is analyzed in this section. Beam with 25.4 mm

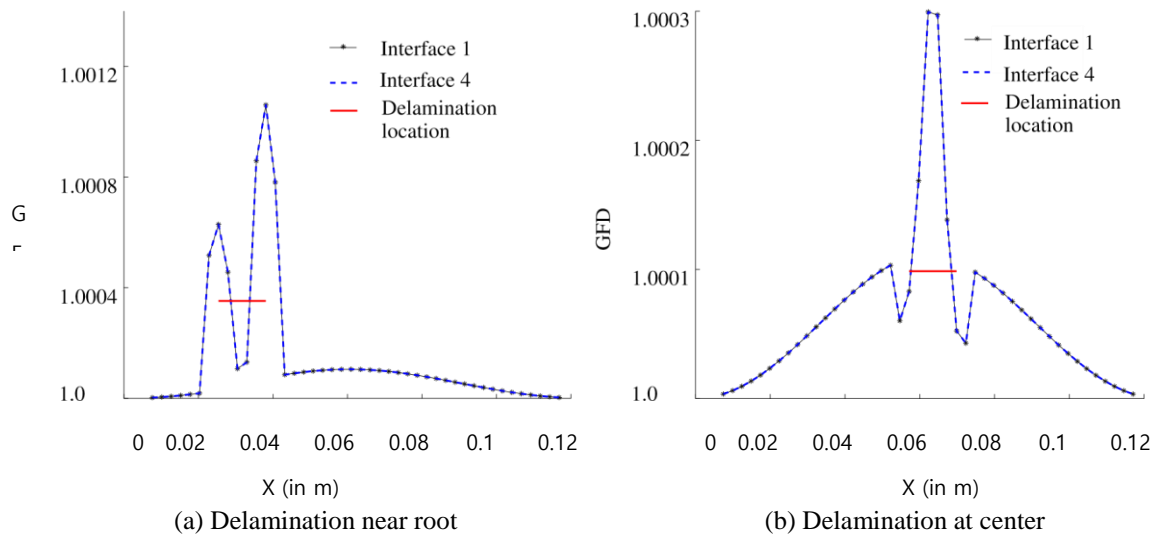


Fig. 13 Effect of the partial width on generalized fractal dimension on torsion mode for fixed-fixed boundary condition

delamination length and full-width delamination in the width-wise direction is considered for the analysis. The fractal dimension curve has a peak at the location of delamination, as seen in Fig. 9.

The effect of change in location of the delamination for simply supported boundary condition on fractal dimension curve is shown in Figs. 9(a) to 9(c). Horizontal line in the figure represents the location and size of delamination in the beam.

Full width delamination in simply supported beam can be detected from the fractal dimension curve. The effect of partial width and simply supported boundary condition on the fractal dimension curve is shown in Fig. 10. Since the simply supported boundary condition problem is symmetric in nature, only two figures corresponding to end and mid delamination location is plotted. Though the location of delamination can be detected from the fractal dimension curve, however, fractal dimension curve for the torsional mode shape may yield better results. Hence, the fractal dimension curve for torsional mode shape data of a simply supported beam is shown in Fig. 11. Partial delamination length of 12.5 mm and 50% width delamination is considered for the simulation.

6.4 Fixed-fixed boundary condition

Effect of delamination location and fixed-fixed boundary condition on the fractal dimension curve is shown in Fig. 12. Delamination length of 25.4 mm and width-wise full width delaminated beam is considered for simulations.

From Fig. 12(a), by looking at the change in fractal dimension curve at the end of delamination, we can predict the presence of delamination, but we cannot say if the delamination is located to the left or right of the sudden change encounter in the fractal dimension curve; same holds true for the Fig. 12(c). In the case of centrally located delamination for the fixed-fixed beam boundary condition, we can confirm the presence of delamination, as there is a drastic change in the fractal dimension curve of the delaminated beams when compared to the healthy beam

fractal dimension curve.

Torsional mode shape of the strip like delaminated beams is affected more, as torsional rigidity reduces drastically in the presence of delamination. Since, the bending mode shape result for fixed-fixed beam is not advantageous for the delamination detection, torsional mode shape may be adopted in detecting the partial delamination in the beam. From the Fig. 13 it is clear that the torsional mode shape can be utilized to detect partial delamination of length 12.5 mm and 50% width delamination in the fixed-fixed beam. The location of the delamination is shown by a horizontal line in the figure.

From the plots it is clear that fractal dimension can be used to detect the delamination in the beam, either by using the first bending mode or the first torsional mode, depending on the size and location of the delamination.

7. Conclusions

A finite element approach is used to study detection of full and partial width delamination in composite beam. An explanation to first natural frequency of delaminated beam being higher than that of the healthy beam for certain delamination lengths and boundary conditions is elaborated. Caution should be exercised if frequency is used as a damage indicator; as also seen in articles Tracy and Pardoen (1989), Hou and Jeronimidis (1999) Detection of delamination in beams using generalized fractal dimension of the mode shape is evaluated. Effect of delamination location on the fractal dimension curve is analyzed for the first bending and the first torsion mode.

The limitations of using generalized fractal dimension for delamination detection are discussed. Delamination in the beam structure can be detected using generalized fractal dimension method using the first few mode shapes. Generalized fractal dimension curve using first bending mode shape data is sufficient to detect delaminations in beams subjected to cantilever boundary conditions. Where as for the beams with simply supported and fixed-fixed

boundary conditions, it is better to use the first torsion mode shape data to calculate generalized fractal dimension curve for successful damage detection.

Fractal dimension method of delamination detection can be used as an efficient way of detecting delamination and can complement other approaches such as those based on wave and NDT methods.

References

- Bai, R., Ostachowicz, W., Radzienski, M. and Cao, M. (2014a), "Vibrational damage detection using fractal surface singularities with noncontact laser measurement". *J. Vib. Control*, 1-13.
- Bai, R.B., Ostachowicz, W., Cao, M.S. and Su, Z. (2014b), "Crack detection in beams in noisy conditions using scale fractal dimension analysis of mode shapes", *Smart Mater. Struct.*, **23**(6).
- Bai, R.B., Song, X.G., Radzienski, M., Cao, M.S., Ostachowicz, W. and Wang, S.S. (2014), "Crack location in beams by data fusion of fractal dimension features of laser-measured operating deflection shapes", *Smart Struct. Syst.*, **13**(6), 975-991.
- Bathe, K.J. (1982), *Finite Element Procedures in Engineering Analysis*. Prentice Hall.
- Cao, M.S., Ostachowicz, W., Bai, R.B. and Radzienski, M. (2013), "Fractal mechanism for characterizing singularity of mode shape for damage detection", *Appl. Phys. Lett.*, **103**, 221906.
- Chandrupatla, T.R. and Belegundu, A.D. (2002), *Introduction to Finite Elements in Engineering*. Pearson Education.
- Chang, F. and Kutlu, Z. (1989), "Response of composite shells containing a delamination", *Appl. Mech. Rev.*, **40**(11), 48-53.
- Della, C.N. and Shu, D. (2007), "Vibration of delaminated composite laminates: A review", *Appl. Mech. Rev.*, **60**(1), 1-20.
- Fan, W. and Qiao, P. (2010), "Vibration-based damage identification methods: A review and comparative study", *Struct. Health Monit.*, **10**(1), 83-111.
- Farhidzadeh, A., Dehghan-Niri, E., Moustafa, A., Salamone, S. and Whittater, A. (2013), "Damage assessment of reinforced concrete structures using fractal analysis of residual crack patterns", *Exp. Mech.*, **53**(9), 1607-1619.
- Gayathri, P., Umesh, K. and Ganguli, R. (2010), "Effect of matrix cracking and material uncertainty on composite plates", *Reliab. Eng. Syst. Saf.*, **95**(7), 716-728.
- Guruprasad, P.J. (2005), Cross-sectional analysis of a pretwisted anisotropic strip in the presence of delamination. Master's thesis, Indian Institute of Science, Bangalore.
- Hadjileontiadis, L.J. and Douka, E. (2007), "Crack detection in plates using fractal dimension", *Eng. Struct.*, **29**, 1612-1625.
- Hadjileontiadis, L.J., Douka, E. and Trochidis, A. (2005), "Fractal dimension analysis for crack identification in beam structures", *Mech. Syst. Signal Pr.*, **19**, 659-674.
- Hakim, S.J.S. and Razak, H.A. (2014), "Modal parameters based structural damage detection using artificial neural networks - a review", *Smart Struct. Syst.*, **14**(2), 159-189.
- Hou, J.P. and Jeronimidis, G. (1999), "Vibration of thin composite plates", *Compos. : Part A*, **30**, 989-995.
- Jefferson, B. and Jarvis, P.R. (2006), *Interface Science in Drinking Water Treatment*, volume 10, Elsevier.
- Jones, R.M. (1999), *Mechanics of composite materials*. Taylor & Francis, 2nd Ed.
- Jun, L., Hongxing, H. and Rongying, S. (2008), "Dynamic finite element method for generally laminated composite beams", *Int. J. Mech. Sci.*, **50**(3), 466-480.
- Katz, M.J. (1987), "Fractals and the analysis of waveforms", *Comput. Biology Medicine*, **18**(3), 145-156.
- Kaveh, A. and Maniat, M. (2015), "Damage detection based on mcss and pso using modal data", *Smart Struct. Syst.*, **15**(5), 1253-1270.
- Keshava Kumar, S., Ganguli, R. and Harursampath, D. (2013), "Partial delamination modeling in composite beams using a finite element method", *Finite Elem. Anal. Des.*, **76**, 1-12.
- Keshava Kumar, S., Ganguli, R. and Harursampath, D. (2015), "Partial delamination detection in rotating beam using generalized fractal dimensions", *Proceedings of the 4th Asian Australian Rotorcraft Forum*.
- Kornev, V.M., Kurguzov, V.D. and Astapov, N.S. (2012), "Fracture model of bimaterial under delamination of elasto-plastic structured media", *Appl. Compos. Mater.*, **20**, 129-143.
- Lee, J. (2001), "Center of gravity and shear center of thin-walled open-section composite beams", *Compos. Struct.*, **52**, 255-260.
- Lee, J. and Kim, S.E. (2001), "Flexural-torsional buckling of thin-walled i-section composites", *Comput. Struct.*, **79**, 987-995.
- Lin, X. and Zhang, Y. (2011), "A novel one-dimensional two-node shear-flexible layered composite beam element", *Finite Element Anal. Des.*, **47**(7), 676-682.
- Moustafa, A. and Salamone, S. (2012), "Fractal dimension-based lamb wave tomography algorithm for damage detection in plate-like structures", *J. Intel. Mat. Syst. Str.*, **23**(11), 1269-1276.
- Pawar, P.M. and Ganguli, R. (2003), "Genetic fuzzy system for damage detection in beams and helicopter rotor blades", *Comput. Method. Appl. M.*, **192**, 2031-2057.
- Prasad, P.S. and Harursampath, D. (2012), "Closed-form nonlinear sectional analysis of pretwisted anisotropic beam with multiple delaminations", *Proceedings of the International Conference on Mechanics of Nano, Micro, Macro Composite Structures (ICMNMCS)*, Torino, Italy.
- Qiao, P., Lestari, W., Shah, M.G. and Wang, J. (2007), "Dynamics based damage detection of composite laminated beams using contact and noncontact measurement system", *J. Compos. Mater.*, **41**(10), 1217-1252.
- Raghavendra, B.S. and Dutt, D.N. (2009), "A note on fractal dimensions of biomedical waveforms", *Comput. Biology Medicine*, **39**, 1006-1012.
- Rahmatalla, S., Eun, H.C. and Lee, E.T. (2012), "Damage detection from the variation of parameter matrices estimated by incomplete fir data", *Smart Struct. Syst.*, **9**(1), 55-70.
- Reddy, J.N. (1997), "On locking-free shear deformable beam finite elements", *Comput. Method. Appl. M.*, **149**, 113-132.
- Senthil, K., Arockiarajan, A., Palaninathan, R., Santhosh, B. and Usha, K.M. (2013), "Defects in composite structures: Its effects and prediction methods - a comprehensive review", *Compos. Struct.*, **106**, 139-149.
- Sheik, A.H. and Thomsen, O.T. (2008), "An efficient beam element for the analysis of laminated composite beams of thin-walled open and closed cross sections", *Compos. Sci. Technol.*, **68**, 2273-2281.
- Shen, M.H.H. and Grady, J.E. (1992), "Free vibrations of delaminated beams", *AIAA J.*, **30**(5), 1361-1370.
- Swanson, S.R. (1998), "Torsion of laminated rectangular rods", *Compo. Struct.*, **42**, 23-31.
- Theiler, J. (1990), "Estimating fractal dimension", *J. Opt. Soc. Am.*, **7**(6), 1055-1073.
- Tracy, J.J. and Pardoen, G.C. (1989), "Effect of delamination on the natural frequencies of composite laminates", *J. Compos. Mater.*, **23**, 1200-1215.
- Umesh, K. and Ganguli, R. (2009), "Shape and vibration control of a smart composite plate with matrix cracks", *Smart Mater. Struct.*, **18**(2), 025002.
- Venkatesh, G., Ponnusami, S.A. and Harursampath, D. (2012), "Delamination studies on composite laminates - an asymptotic approach", *Proceedings of the European solid mechanics conference*, Graz, Austria.
- Wang, J. and Qiao, P. (2007), "Improved damage detection for beam-type structures using a uniform load surface", *Struct.*

Health Monit., **6**(2), 99-110.

- Xiang, J., Nackenhorst, U., Wang, Y., Jiang, Y., Gao, H. and He, Y. (2014), "A new method to detect cracks in plate-like structures with through-thickness cracks", *Smart Struct. Syst.*, **14**(3), 397-418.
- Zou, Y., Tong, L. and Steven, G. (2000), "Vibration-based model-dependent damage (delamination) identification and health monitoring for composite structures - a review", *J. Sound Vib.*, **230**(2), 357-378.

CY

